3-D reverse VSP

Zandong Sun and Robert R. Stewart

ABSTRACT

3-D reverse VSP is a novel way to create a 3-D image around a borehole. A 3-D numerical modeling experiment with three-component (3-C) receivers is implemented here by raytracing through a model consisting of three layers with a dome on the top of second layer. We find that the converted-wave (P-SV) has wider coverage than P-P wave, and allows us to image more highly dipping reflectors than P-P waves do. The dome in the model with reflector dip angle variation of 0° to 36.9° (dipping away from the borehole) can be 60-70% imaged by the P-SV wave, but can only be imaged 30-40% by the P-P wave. For a flat interface, 75% of the source-receiver offset from borehole can be imaged by P-SV(V_P/V_S ratio dependent) wave while P-P wave can only image 50%. Practically, for a source-receiver offset of 2500 meters, the P-SV wave can image reflector of dip angle of 30° while P-P wave can only image 20° in both cases that reflector dips away from borehole. We outline an analysis flow for the processing of 3-D reverse vertical seismic profile (RVSP) data. The proposed processing flow includes static removal, several methods of velocity analysis and binning, stacking, and migration.

INTRODUCTION

In situ seismic measurements (VSP and crosswell) have proven useful for imaging and estimating rock properties near or between wells. However, it is generally very expensive or impractical to extend either measurement into a full three-dimensions (3-D). Because the earth is generally heterogeneous in three dimensions and our regions of interest are usually volumetric, 3-D images are critical. The reverse VSP (RVSP) operates using downhole sources and surface receivers. Because we can often inexpensively deploy an areal grid of surface geophones, the potential arises for full 3-D data recorded from downhole shots. In the 2-D case, a single line of geophones receives energy from downhole sources. A number of authors have recently considered the analysis of 2-D RVSP data (Jackson et al., 1989; Jones, 1991; Kragh et al., 1991; Naville et al., 1991; Hardage, 1992; Parra and Bangs, 1992). Haldorsen et al. (1992) used several 2-D surface lines to image data recorded from a downhole drill-bit source. Their drill-bit seismic image matched surface seismic and conventional walkaway VSP images reasonably well. Aleotti et al. (1994) also showed drill-bit images (prediction ahead of the bit seismograms) that were similar to synthetic seismograms produced from logs after the well had been drilled through the predicted depths. Chen and McMechan (1992) considered the 3-D case and used synthetic data from a salt structure model to perform a 3-D pre-stack depth migration. They showed that 2-D analysis produced artifacts while the 3-D algorithms provided a much more accurate picture.

In this work, we address the advantages and limitation of 3-component 3D reverse VSP through ray-tracing a numerical model by comparing compressional-wave (P-wave) and converted-wave (P-SV wave). We are developing 3-D reverse VSP

depth-variant binning, and we propose development of procedures for the handling and processing of model and field 3-D RVSP data.

RAY-TRACING AND NUMERICAL MODELING

Model description and receiver array

A plan view of the model, 3500 meters by 3000 meters, is shown in Figure 1a. There are 61 receiver lines oriented East-West (E-W) - the inline direction - with a 50 meter line spacing from 0 to 3000 meters along North-South (N-S) direction (the crossline direction). The coordinate system is defined in the convention of (N-S, E-W) on the 2-D horizontal plane. There are 61 receivers per line with 50 meters receiver spacing. The array plot in Figure 1a shows every other receivers on every other receiver lines.

The model consists of three layers (Figure 1b) which was built using SIERRA MIMIC software package. The thickness of three layers from top to bottom are 800 m, 400 m, and 800 m respectively. A dome centered at (1500, 1500) is located on the top of second layer with radius of 630 m and height of 210 m, which possesses dip angles varied from 0° to 36.9° (after some math operation). The physical properties of these three layers are listed in Table 1.

Table 1. Physical properties of the numerical model

Layer	Velocity (m/s)		V_p/V_s	Poisson's Ratio	Density	Q factor	
	V_p	V_s				Q_p	Q_s
1	4000	2000	2.0	0.33	2.60	309	137
2	5200	2600	2.0	0.33	2.96	546	243
3	6400	3695	1.73	0.25	3.50	864	384
half space	7620	4399	1.73	0.25	2.89	1273	365

Ray-tracing and results

P-P and P-SV ray-tracing through the model was implemented using the SIERRA 3-D QUIKVSP package. P-P reflections and P-SV reflections from the top of second and third layer, and direct arrivals are defined in the ray instruction. The model was shot at source depth varied from 1200 m to 0 m with total of 31 shots at two different surface well locations (A) (1500,1500) and (B) (2200,1500) (assuming that the well hits the target and misses the target). Surface receivers array with total of 3721 channels (61by 61) per shot record are recording simultaneously.

Raypath plots to be shown were sampled on every other receivers in both the inline and crossline directions. Raypath view angles are defined by two parameters ø

and ß. The angle ø is defined as the angle between the dip plane and a horizontal plane with positive value when dipped downward and negative value when dipped upward, e.g. ø equals to zero for a horizontal plane. The angle ß is defined as the angle between model N-S axes and true north direction with positive value when clockwise, e.g. ß equals to zero for true north direction. We use the expression (ø,ß) for viewing angles. Figure 2 shows P-P reflection raypath (the front ray set is taken away for better visualization) and P-P coverage at viewing angles (0°,0°) when model is shot at depth of 0.0 m (source located on surface), in which case the plot shows the most P-P coverage on both dome and flat interface. As stated above, the dip angle of the dome varies from 0° (at the very top of the dome) to 36.9° (at the edge of the dome connecting the flat interface). Overall, half distances of maximum source receiver offsets are covered from all azimuths. However, the dome was only covered 30-40%. As the source moves down the borehole, the P-P coverage becomes smaller on both the dome and flat interface. Figure 3 shows the P-P raypath plot viewed at the same angle when model is shot at source depth of 200 m. These indicate the closer to the borehole the higher the fold coverage.

The P-SV raypath plot for source depth of 0.0 m (source located at surface) is shown in Figure 4. Apparently, converted-wave events have much wider coverage on both the dome and flat interface with the same receiver array (both 2-D and 3-D space, see Figure 5 and Figure 6). The dome is covered around 60-70%. A flat interface can be covered as much as 75% distance of maximum source-receiver offset on all azimuth direction. At this stage, we can draw two conclusions: (a) 3-D reverse VSP P-SV wave has wider coverage than the P-P wave, and it allows us to image a more dipping reflector than P-P wave does; (b) unlike the normal VSP where P-SV coverage is narrower than P-P wave in the 3-D reverse VSP, the converted-wave coverage is larger.

What is the raypath (coverage) if the well misses the target (dome)? The other well location (B) (2200,1500) was proposed and the model was shot through various source depths. Ray-tracing plots described above shows the case in which the reflector dips away from borehole in all azimuth direction. We now consider the case in which the reflector first dip towards the borehole and then dip away from the borehole. The P-P raypath plot for source located at the top (surface) of well B is shown in Figure 7, viewed at view angle (0°,90°), which shows the maximum coverage of 3-D RVSP at such well location. Half the distance of the source-receiver offset is covered for a flat interface, and the dome coverage is about 50-60%. One side of dome edge (close to well) can be imaged. Figure 8 shows P-SV raypath plot (one ray set taken away for visualizing outline of the dome) , viewed at angle (0°,90°), for source located at depth of 200 m in the well B. Not only has it wider coverage than previous plot in which case source was located on surface, but also 70-80% of dome surface is covered!

One should be reminded that all the raytracing plots shown above are viewed in 3-D space. It seems that many different reflection locations were recorded on one receiver (especially on Figure 4 and 8). As a matter of fact, each surface location shown on a raypath plot is a receiver line, crossline direction when viewed at angle (0°,0°) and inline direction when viewed at angle (0°,90°).

RVSP OFFSET AND DIP ANGLE FOR P-P AND P-SV WAVES

We now consider source-receiver offset and reflector dip angle for 3-D reverse VSP, and derive the formula for minimum offset requirement when certain coverage of

a target is required in the case of reflector dip away from borehole. This consideration does not include the Fresnel zone. The Fresnel zone for both P-P and P-SV wave in either surface case or VSP case can be calculated by following the work by Eaton et al. (1991).

The P-SV wave is first considered. Usually we know the depth of the target through the drilling, and the source depth is always a known (S_d); therefore, the distance from source to the target (K) is a known. The dip angle (θ) can be estimated from migrated surface seismic section. Showing in Figure 9, we can denote the horizontal distance between wellbore and far side edge of the target as L, and minimum source-receiver offset as X_{min}. According to Snell's law, P-wave incident angle i and S-wave converted angle j are related as:

$$\sin j = \frac{V_s}{V_p} \sin i \tag{1}$$

where V_S and V_P are the average velocities for S-wave and P-wave at target depth. Using the triangle relationship in Figure 9, we build the following equation:

$$X_{min} = \frac{\left(\frac{K \cos\theta}{\sin(\pi/2 - i)} + \frac{Sd}{\cos(\theta - i)}\right)\sin(i+j)}{\cos(\theta + j)} - \frac{K \cos\theta}{\sin(\pi/2 - i)} \tag{2}$$

After some math operations (delta functions), we have the following expressions:

$$X_{min} = K \frac{\gamma \cos\theta}{\cos i} + S_d \frac{\gamma + \sin(\theta - i)}{\cos(\theta - i)} \tag{3}$$

where γ is the function of incident angle (i), conversion angle (j), and reflector dip angle (θ) defined by the following equation:

$$\gamma = \frac{\sin(i+j)}{\cos(\theta + j)} \tag{4}$$

The incident angle can be defined by the distance from source to the target (K), the horizontal distance between wellbore and far side edge of the target (L), and the dip angle (θ) as follow:

$$\cos i = \frac{K \cos^2\theta \sqrt{K^2\cos^2\theta + L^2 + KL\sin(2\theta)}}{K^2\cos^2\theta + L^2 + KL\sin(2\theta)} \tag{5}$$

A similar formula for P-P wave can be easily obtained when conversion angle j is replaced by i, in which case the θ function is expressed as follow:

$$\gamma = \frac{\sin(2i)}{\cos(\theta + i)} \tag{6}$$

As we have discussed in raytracing, for 3-D reverse VSP the coverage reaches maximum when source is located on the top of a well. Assuming a target depth (K) 2000 meters, source on the top of a well (S_d equals to 0 m), and V_P/V_S 2.0, we have calculated crossplots of minimum source-receiver offset (The Fresnel zone not included yet) and horizontal distance of subsurface image at various reflector dip angle (dip away from borehole) for both P-P and P-SV waves (Figure 10 and 11). Downhole source energy has to be high enough if offset is 2500 meters. For a surface receiver array with maximum offset of 2500 meters (5000 meters cross the receiver line) P-P wave can probably image 2350 meters (The Fresnel zone roughly considered) if reflector is flat (D.A.=0°), 1350 meters if reflector dip angle is 10°, 450 meters if reflector dip angle is 20°. However, P-SV wave has much better coverage. For the same surface receiver array, P-SV can probably image 3450 meters if reflector is flat, 2400 meters if reflector dip angle is 10°, 1400 meters if reflector dip angle is 20°, 330 meters if reflector dip angle is 30°. Again, the Fresnel zone is roughly considered. The reflector with dip angle of 40° can not be imaged. The reflector dipping towards borehole can be better imaged.

PROCESSING

There are a number of steps required to process RVSP data. Included are statics removal, velocity analysis, wavetype separation, mapping, stacking, and migration. We could estimate receiver statics from deep shots or perhaps use the surface seismic estimated values. We also need to remove the direct arriving waves to allow better imaging using the reflected events. Separation of the direct and reflected events might be assisted by using data grouped in ways other than by common shot(s) or receiver(s). However, conventional median or f-k filters on common receiver gathers are likely to be adequate. Useful possible gathers include constant s-r groups or s+r groups. We intend next to develop a fast method to remove NMO and stack the data. There are two possible methods to accomplish this: i) a VSPCDP map type of process or, ii) a CRP-type gather with stacking velocity analysis, NMO removal, and stack. Using this approximate stack structure and prior velocity values, we could go back and do the full pre-stack migration. The pre-stack migration could be accomplished using a reverse-time algorithm, Kirchhoff implementation, or other procedure that allows source and receiver to be a very different elevations. We could upward continue the shot data to make the raw RVSP look like 3-D surface seismic data, then process the whole continued RVSP as a standard 3-D survey. Or similarly, we could downward continue the surface recordings to their shot depths, then handle each shot as a layer stripped surface seismic data set. After migrating each shot, the images could be stacked. The downward continuation methods may be the most effective. We intend to interpret the data using conventional 3-D interpretation methods on the processed volumes. Various sections and time slices will be formed. The processing flow we are following is shown in Table 2.

Figure 12 shows common shot record of three receiver lines (inline) from the numerical modeling with sources depth of 1200 m to 0 m (40 m shot interval) located in Well A . There are 31 shot records acquired. The whole data volume is sorted to common receiver domain (see Figure 13). The median filter is employed for wavefield separation, and it performs well (Figure 14).

As stated above, the P-SV wave image is quite promising in 3-D reverse VSP surveying. The wavefield separation will then become a critical issue

Table 2. 3-D reverse VSP processing flow

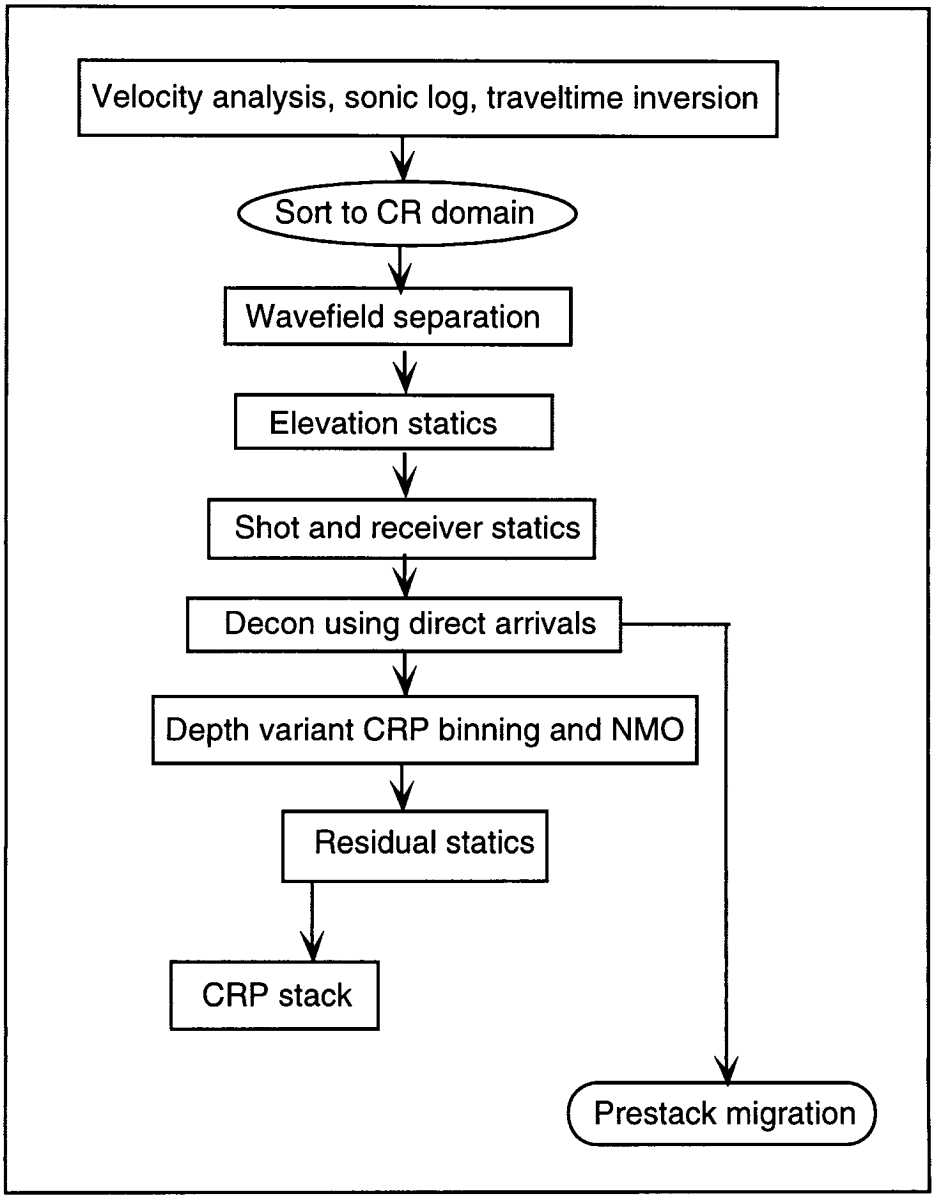

At this stage, the analytical binning algorithm is used for 3-D RVSP binning. P-P wave binning algorithm is summarized in Table 3.

Table 3. 3-D reverse VSP P-P wave binning and NMO flowchart

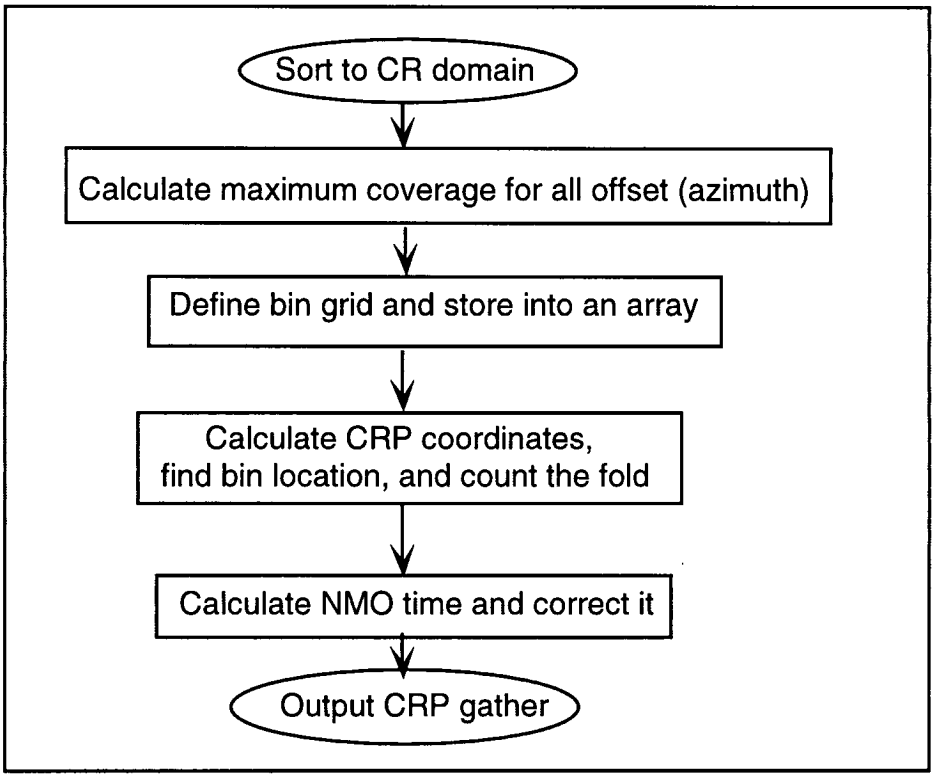

CONCLUSIONS

This preliminary study has shown that the 3-D RVSP P-SV wave has wider coverage than the P-P wave, and it allows us to image a more dipping reflector than the P-P wave does, which contrasts 3-D RVSP from normal VSP (P-SV wave coverage is narrower than P-P wave). Therefore, in the 3-D RVSP survey, P-SV wave image may be very useful.

REFERENCES

Aleotti, L., Gallori, A., Miranda, F., Craglietto, A., Persoglia, S., Poletto, F., Impact of drill-bit seismic method on explorative wells: Presented at the **56**th Ann. Mtg., Europ. Assn. Explor. Geophys., Vienna.

Chen, H. and McMechan, G.A., 1992, 3-D pre-stack depth migration for salt and subsalt structures using reverse-VSP data: J. Seis. Expl., **1**, 281-291.

Eaton, W. S. D., Stewart, R. R., and Harrison, M. P., 1991, The Fresnel zone for P-SV waves: Geophysics **56**, 360-364.

Haldorsen, J. B. U., Miller, D. E., Walsh, J. J., and Zoch, H.-J., 1992, Multichannel approach to signature estimation and deconvolution for drill bit imaging: Presented at the **62**nd Ann. Intl. Mtg., Soc. Explor. Geophys., New Orleans.

Hardage, B.A., 1992, Reverse VSP and crosswell seismology: Geophysical Press.

Jackson, P.J., Onions, K.R., and Westerman, A.R., 1989, Use of inverted VSP to enhance the exploration value of boreholes: First Break, **7**, 233-246.

Jardine, D. 1974, Cretaceous oil sands of Western Canada: CSPG Memoir **3**, 50-67.

Jones, M., 1991, On the analysis of a reverse VSP data set using a core-gun source: Presented at the Sixty-First Ann. Intl. Mtg. Soc. Expl. Geophys., Houston.

Kragh, J.E., Goulty, N.R., and Findlay, M.J., 1991, Hole-to-surface seismic reflection surveys for shallow coal exploration: First Break, **7**, 335-344.

Minken, F.D., 1974, The Cold Lake Oil Sands: Geology and a reserve estimate: CSPG Memoir **3**, 84-89.

Naville, C., Layotte, P.C., Serbutoviez, S., and Verdier, F., 1991, Uphole surveys digitally recorded and processed as multi-offset RVSP's: Presented at Ann. Mtg. Europ. Assoc. Expl. Geophys., Paris.

Parra, J. O. and Bangs, J. H., 1992, High-resolution reverse VSP and interwell seismic experiments at the Buckhorn test site in Illinois: Presented at the **62**nd Ann. Intl. Mtg., Soc. Explor. Geophys., New Orleans.

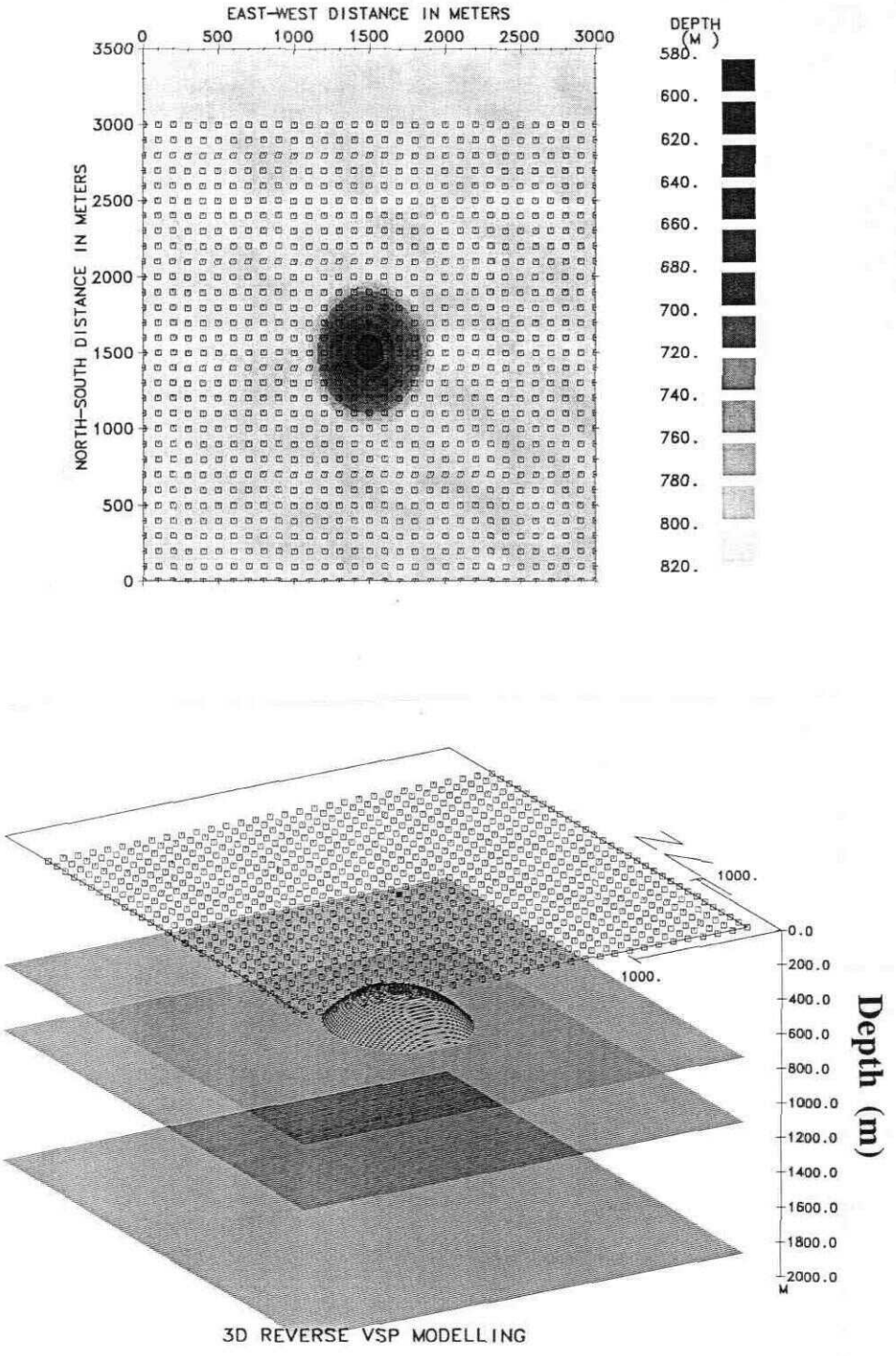

FIG. 1. Geometry of 3-D RVSP numerical model: a) plane view of receiver array (plotted 100 m spacing) and depth of the top of second layer; Well "A" is located at North-south 1500 m and East-west 1500 m, well "B" is located North-south 2200 m and East-west 1500 m; b) 3-D prospective plot of the model.

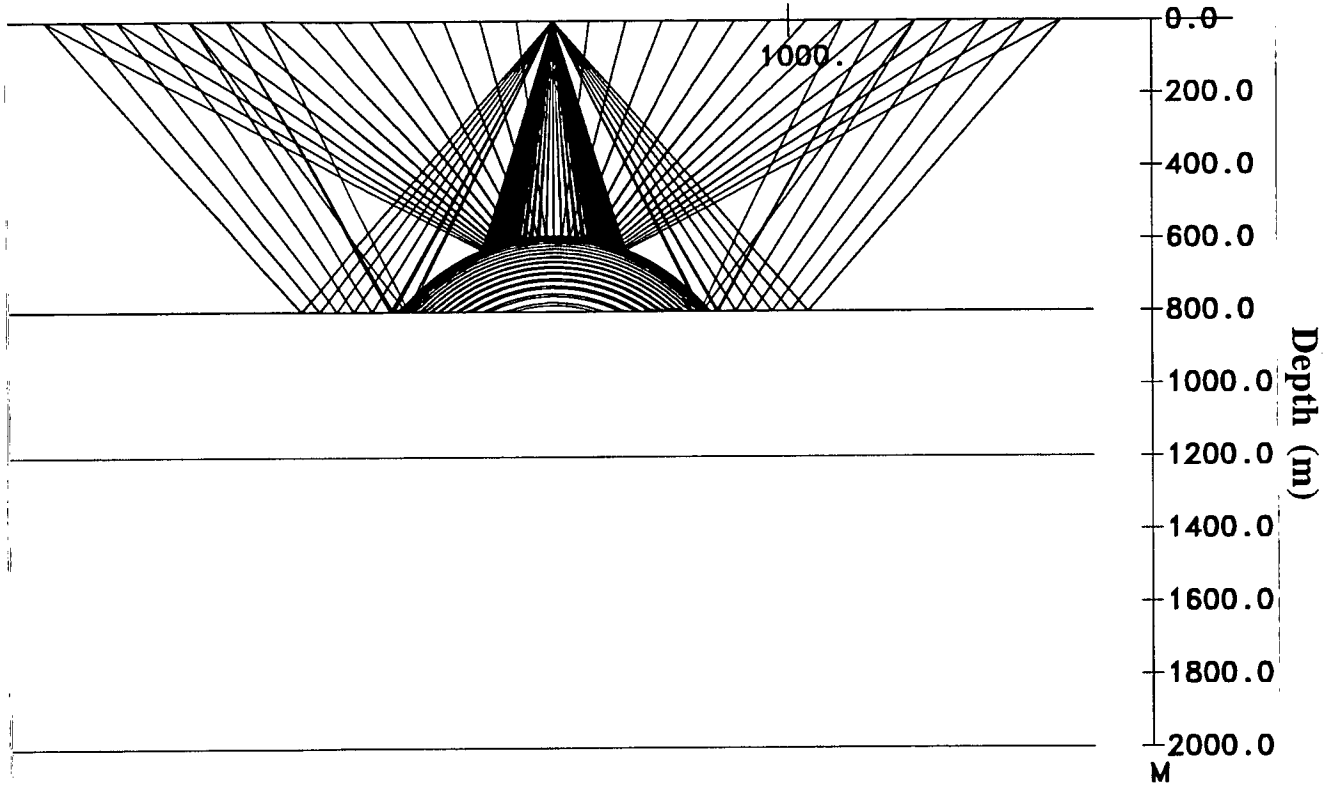

FIG. 2. Raytracing plot of P-P wave for case of reflector dipping away from borehole showing P-P reflection raypath (the front ray set turned off for better visualization) and P-P coverage at viewing angles (0°,0°) with source depth of 0.0 m (source located on surface) in Well "A". The first viewing angle is defined as the angle between the dip plane and a horizontal plane e.g. 0° presents horizontal plane; the second viewing angle is defined as the angle between model N-S axes and true north direction.

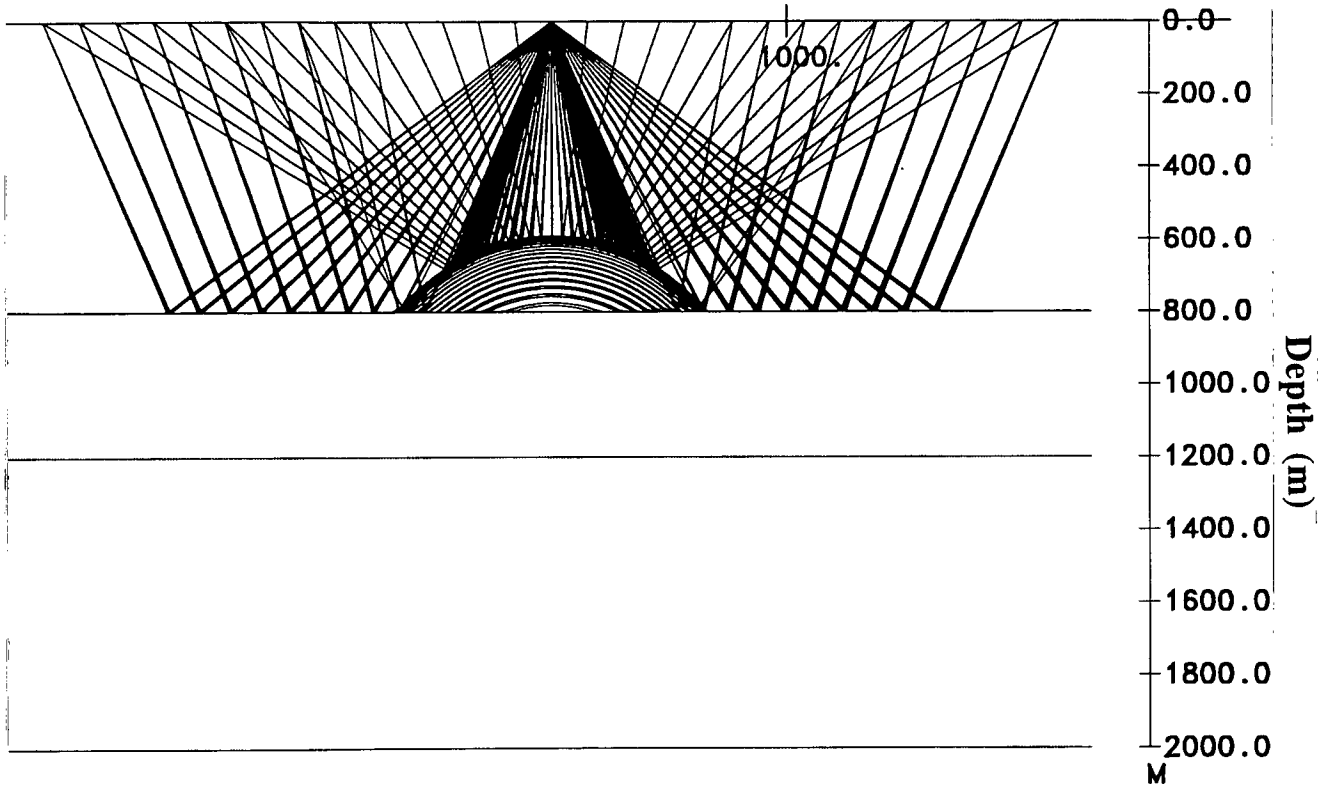

FIG. 3. Raytracing plot of P-P wave for case of reflector dipping away from borehole showing P-P reflection raypath and P-P coverage at viewing angles (0°,0°) with source depth of 200.0 m in Well "A". The first viewing angle is defined as the angle between the dip plane and a horizontal plane e.g. 0° presents horizontal plane; the second viewing angle is defined as the angle between model N-S axes and true north direction.

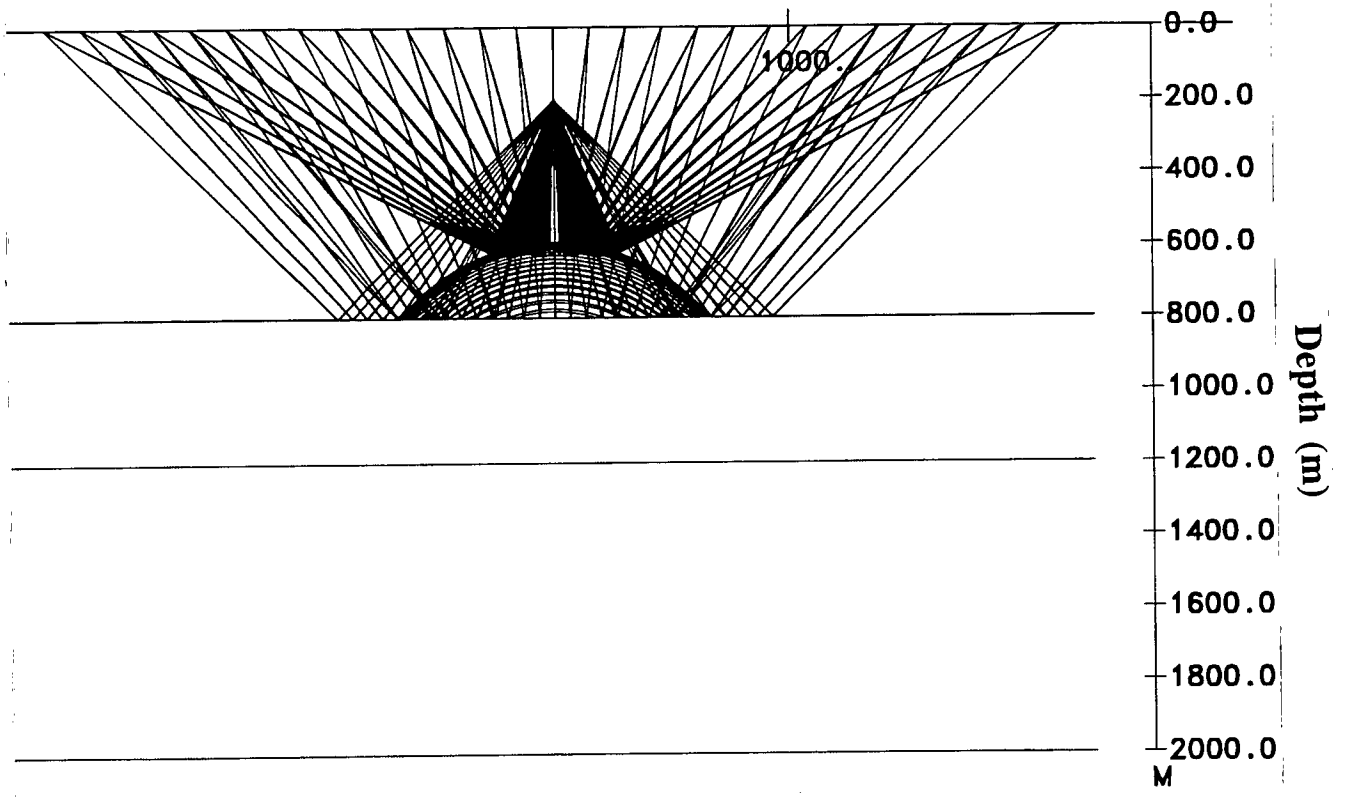

FIG. 4. Raytracing plot of P-SV wave showing P-P reflection raypath (the front ray set turned off for better visualization) and P-SV coverage at viewing angles (0°,0°) with source depth of 0.0 m (source located on surface) in Well "A". The first viewing angle is defined as the angle between the dip plane and a horizontal plane e.g. 0° presents horizontal plane; the second viewing angle is defined as the angle between model N-S axes and true north direction.

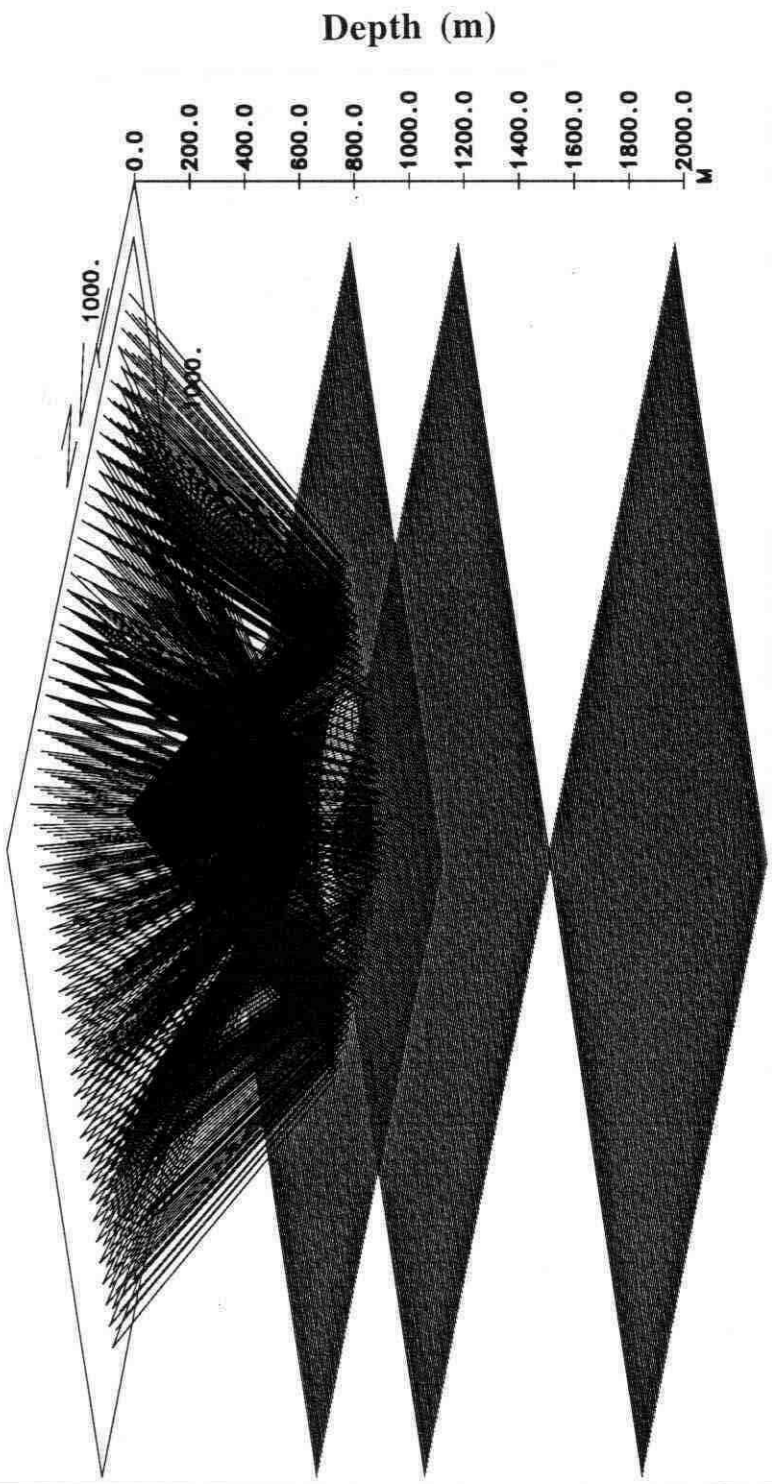

FIG. 5. Overall P-P wave coverage plot for source located in Well "A" at surface.

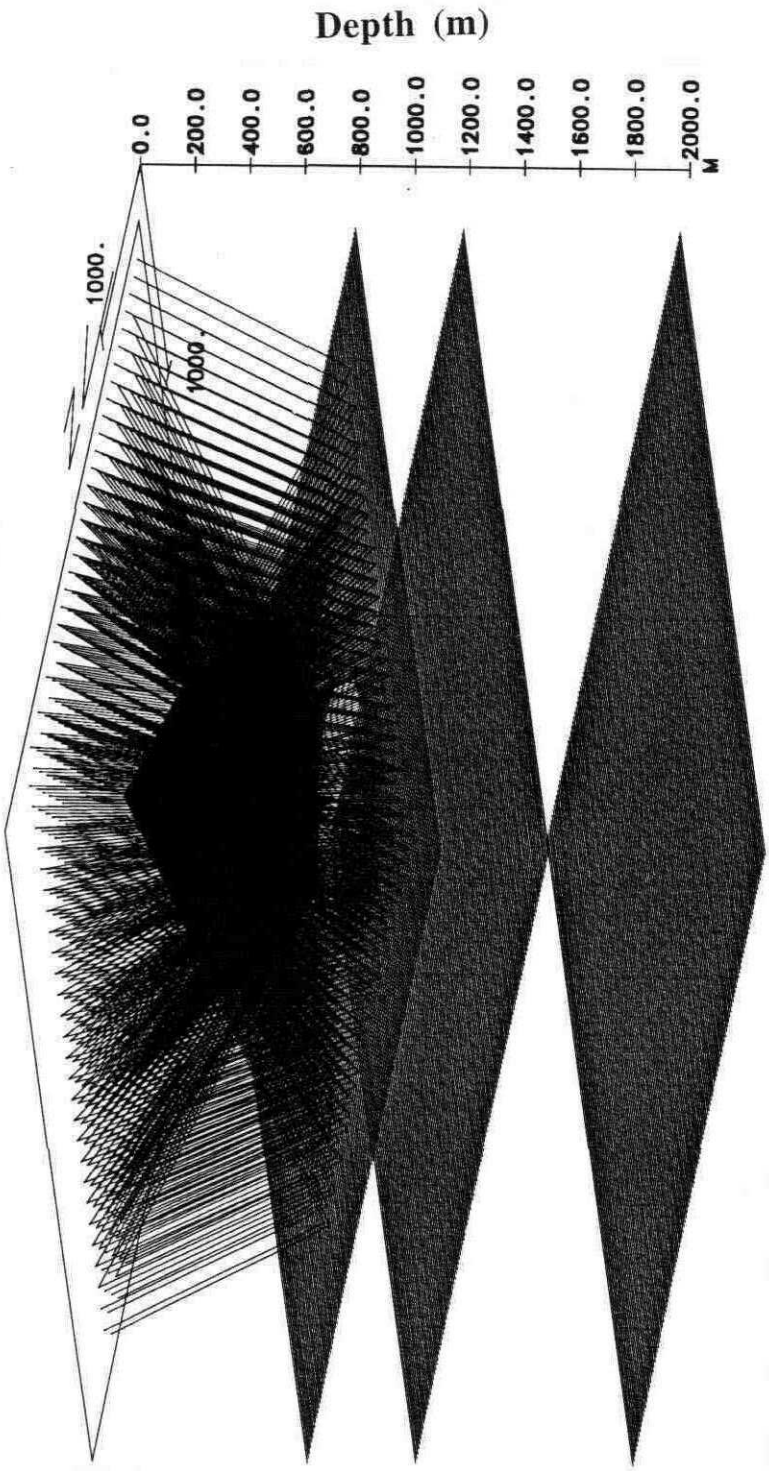

FIG. 6. Overall P-SV wave coverage plot for source located in Well "A" at surface.

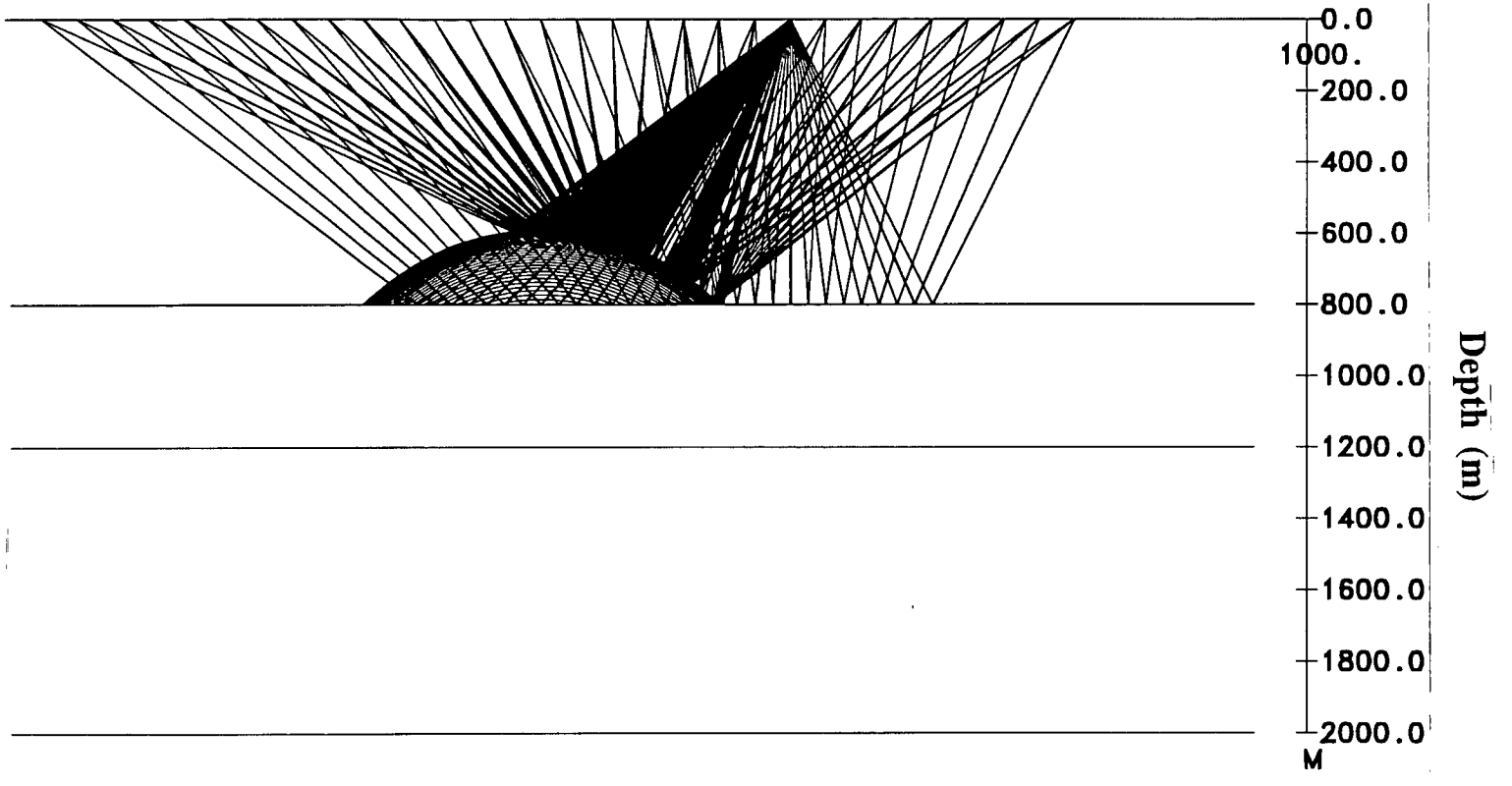

FIG. 7. Raytracing plot of P-P wave for case of reflector dipping towards borehole showing P-P reflection raypath and P-P coverage at viewing angles (0°,90°) with source depth of 0.0 m (source located on surface) in Well "B". The first viewing angle is defined as the angle between the dip plane and a horizontal plane e.g. 0° presents horizontal plane; the second viewing angle is defined as the angle between model N-S axes and true north direction.

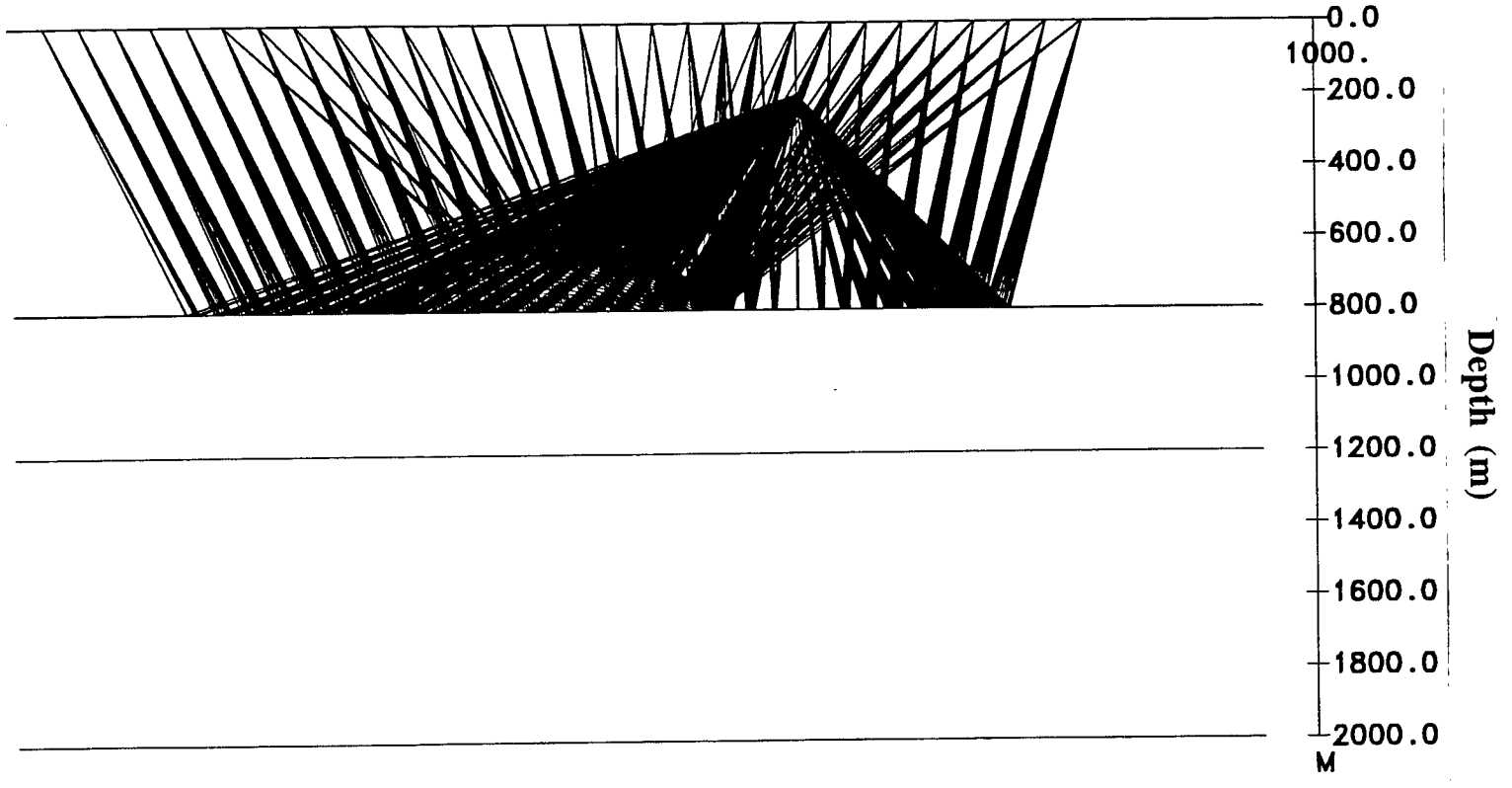

FIG. 8. Raytracing plot of P-SV wave for case of reflector dipping towards borehole showing P-SV reflection raypath and P-SV coverage at viewing angles (0°,90°) with source depth of 200.0 m in Well "B". The first viewing angle is defined as the angle between the dip plane and a horizontal plane e.g. 0° presents horizontal plane; the second viewing angle is defined as the angle between model N-S axes and true north direction.

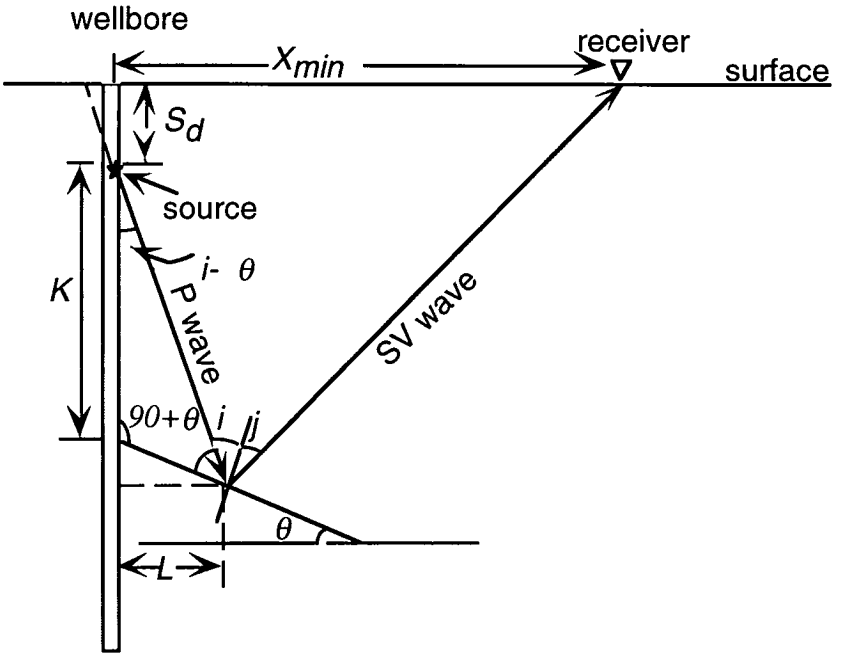

FIG. 9. Geometry and symbols used for calculation of minimum offset.

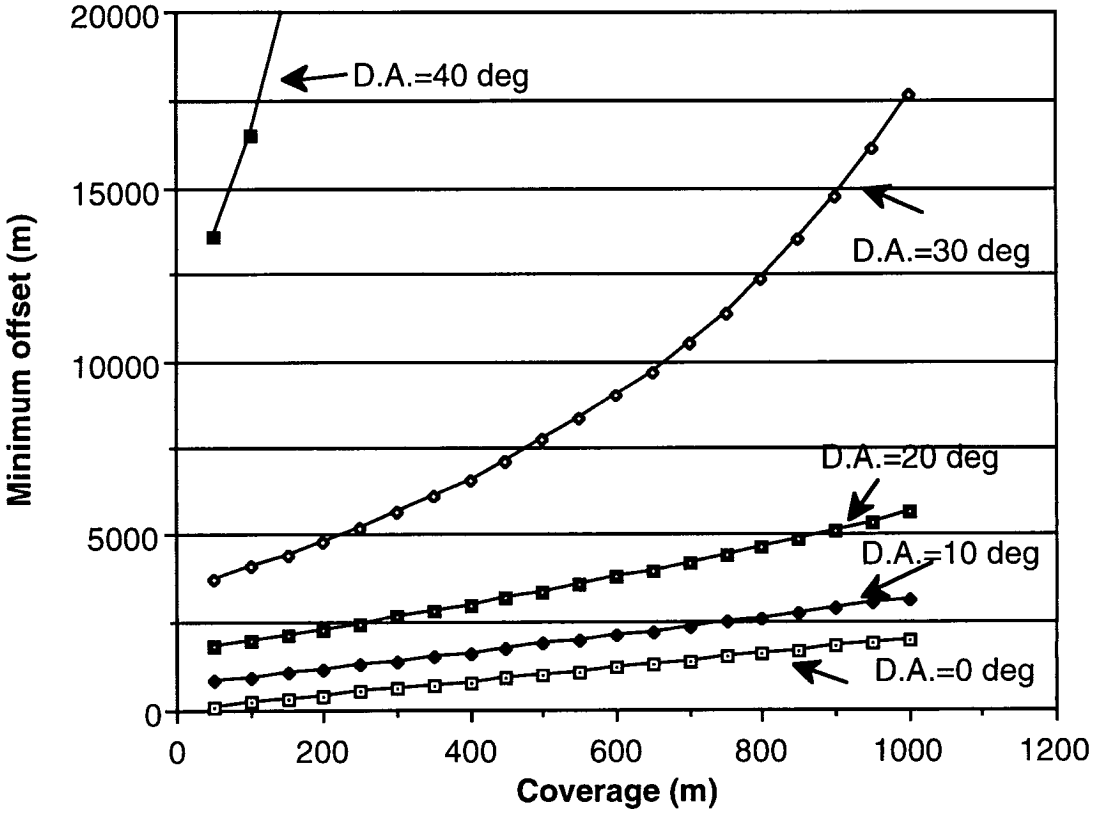

FIG. 10. Crossplot of P-P wave reflection coverage and minimum offset required with various reflector dip angle (D.A.).

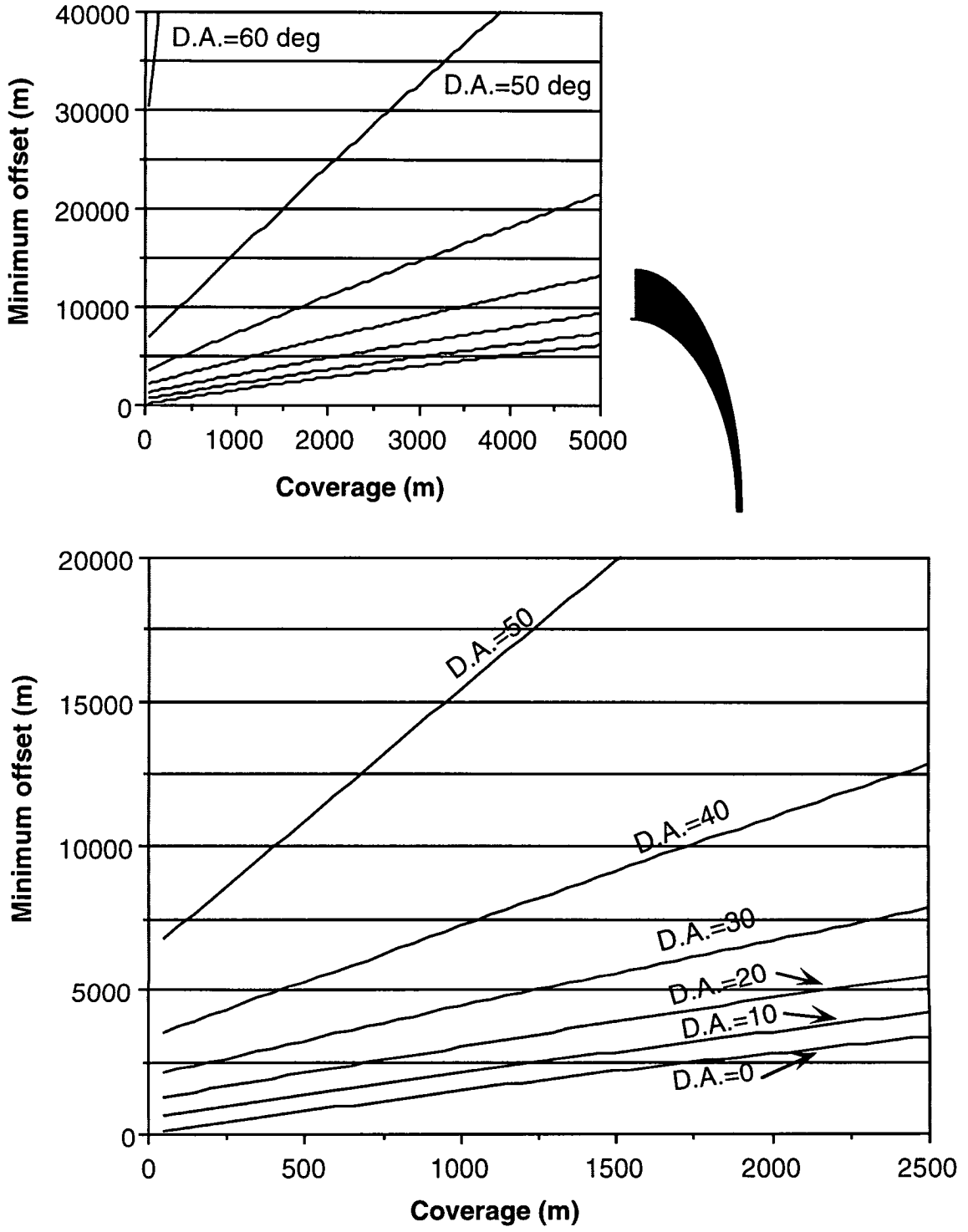

FIG. 11. Crossplot of P-SV wave reflection coverage and minimum offset required with various reflector dip angle (D.A.).

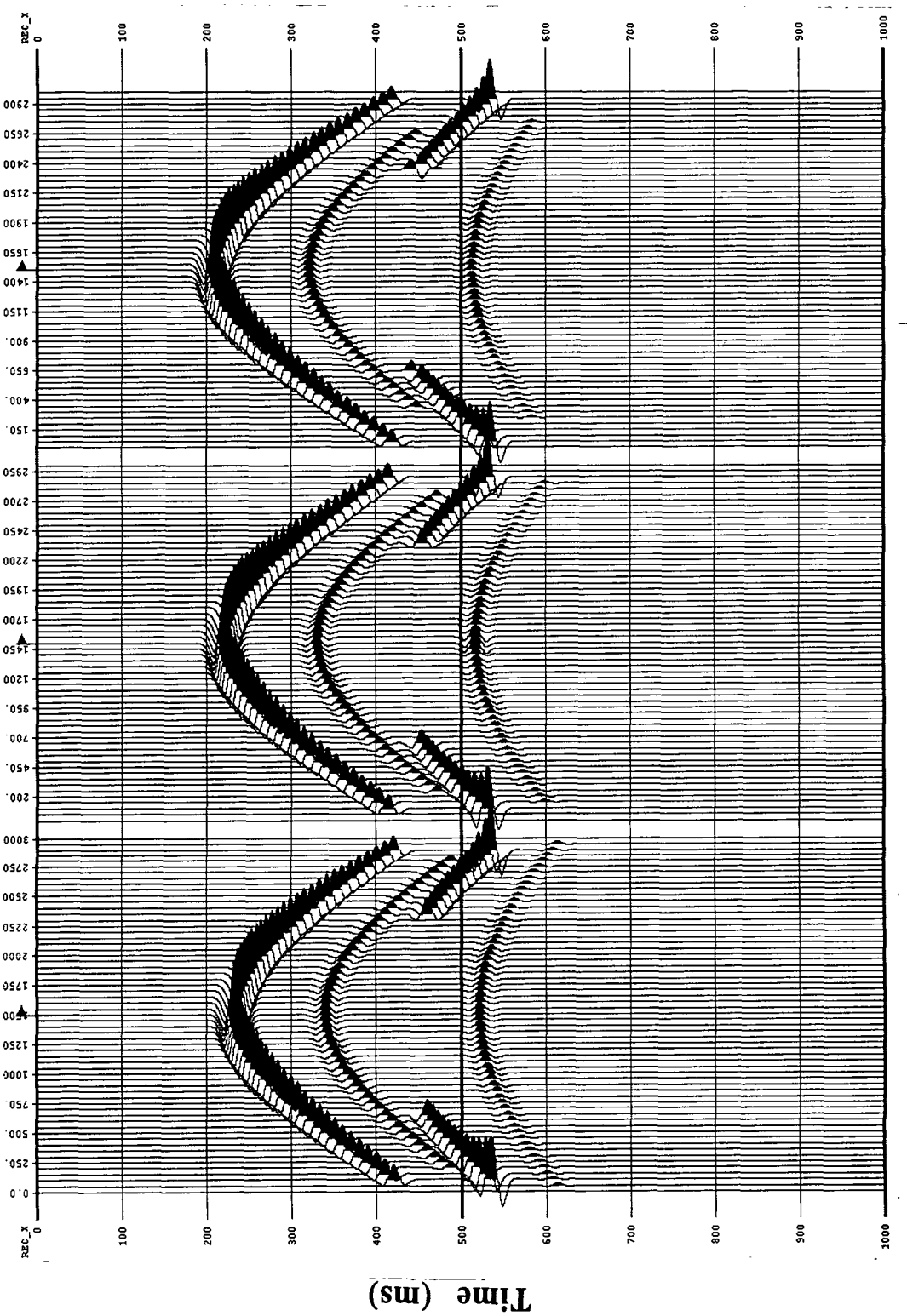

FIG. 12. Common shot record of three receiver lines from numerical modeling.

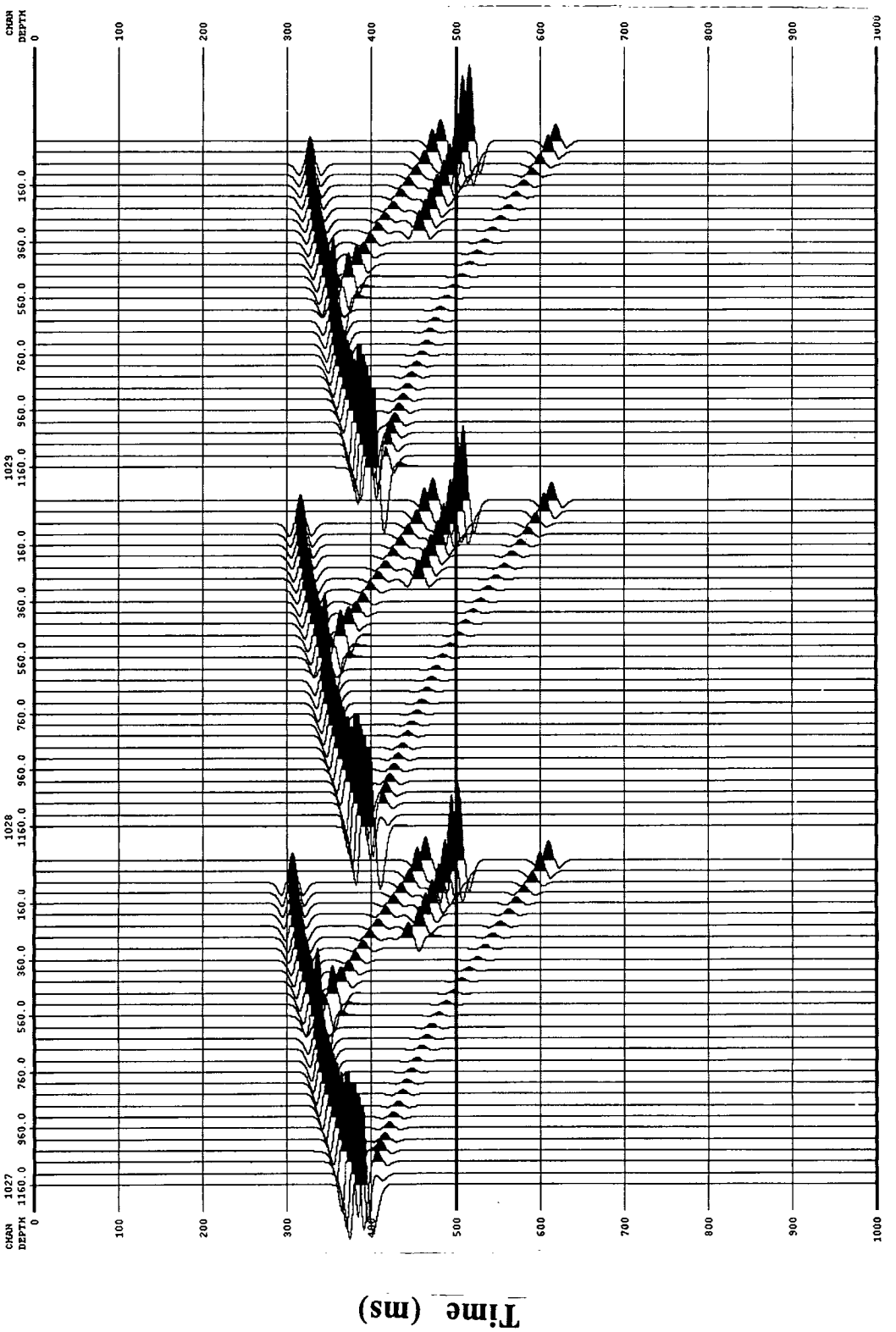

FIG. 13. Common receiver record of three channels.

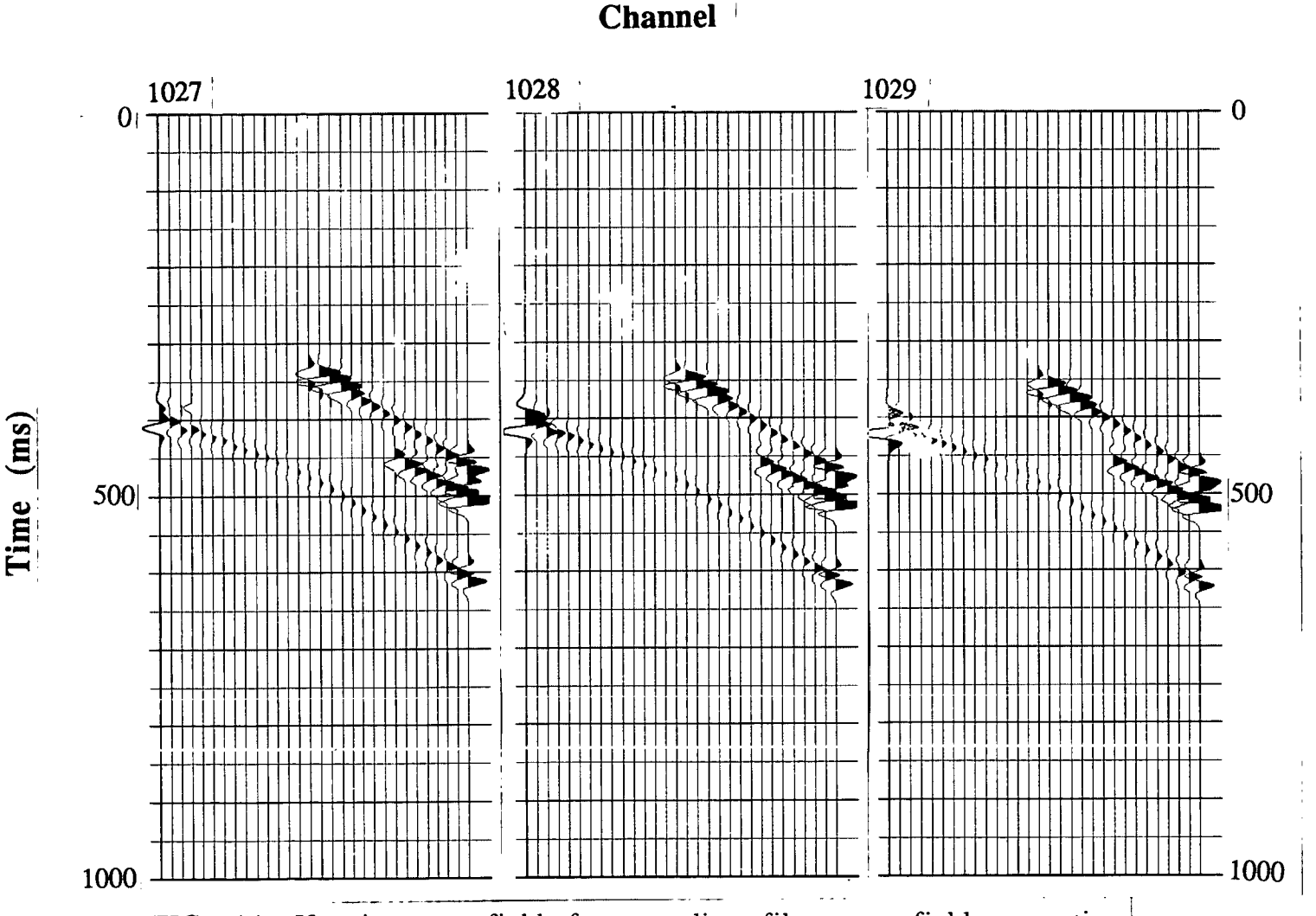

FIG. 14. Upgoing wavefield from median filter wavefield separation.